Angular Differential Imaging: a Powerful High-Contrast Imaging Technique
— Source link ⧉

Christian Marois, Christian Marois, David Lafrenière, René Doyon ...+2 more authors

Institutions: Université de Montréal, Lawrence Livermore National Laboratory

Published on: 10 Apr 2006 - The Astrophysical Journal (IOP Publishing)

Topics: Speckle noise, Speckle pattern, Adaptive optics, Field of view and Gemini Planet Imager

Related papers:

- Detection and characterization of exoplanets and disks using projections on karhunen-loève eigenimages

- A New Algorithm for Point-Spread Function Subtraction in High-Contrast Imaging: A Demonstration with Angular Differential Imaging

- Direct imaging of multiple planets orbiting the star HR 8799.

- Evolutionary models for cool brown dwarfs and extrasolar giant planets. The case of HD 209458

- Evolutionary models for cool brown dwarfs and extrasolar giant planets. The case of HD 20945

Angular Differential Imaging: a Powerful High-Contrast Imaging Technique

C. Marois, D. Lafreniere, R. Doyon, B. Macintosh, D. Nadeau

November 9, 2005

Disclaimer

Angular Differential Imaging: a Powerful High-Contrast Imaging Technique [1]

Christian Marois[2,3], David Lafrenière[2], René Doyon[2], Bruce Macintosh[3],

Daniel Nadeau[2]

[2] *Département de physique and Observatoire du Mont Mégantic, Université de Montréal,*

C.P. 6128, Succ. A,

Montréal, QC, Canada H3C 3J7

[3] *Institute of Geophysics and Planetary Physics L-413,*

Lawrence Livermore National Laboratory, 7000 East Ave, Livermore, CA 94550

cmarois@igpp.ucllnl.org david@astro.umontreal.ca doyon@astro.umontreal.ca

bmac@igpp.ucllnl.org nadeau@astro.umontreal.ca

ABSTRACT

Angular differential imaging is a high-contrast imaging technique that reduces speckle noise from quasi-static optical aberrations and facilitates the detection of faint nearby companions. A sequence of images is acquired with an altitude/azimuth telescope, the instrument rotator being turned off. This keeps the instrument and telescope optics aligned, stabilizes the instrumental PSF and allows the field of view to rotate with respect to the instrument. For each image, a reference PSF obtained from other images of the sequence is subtracted. All residual images are then rotated to align the field and are median combined. Observed performances are reported for Gemini Altair/NIRI data. Inside the speckle dominated region of the PSF, it is shown that quasi-static PSF noise can be reduced by a factor ∼5 for each image subtraction. The combination of

all residuals then provides an additional gain of the order of the square root of the total number of images acquired. To our knowledge, this is the first time an acquisition strategy and reduction pipeline designed for speckle attenuation and high contrast imaging is demonstrated to significantly get better detection limits with longer integration times at all angular separations. A PSF noise attenuation of 100 was achieved from 2-hour long sequences of images of Vega, reaching a 5-sigma contrast of 20 magnitudes for separations greater than $7''$. This technique can be used with currently available instruments to search for ~ 1 M_{Jup} exoplanets with orbits of radii between 50 and 300 AU around nearby young stars. The possibility of combining the technique with other high-contrast imaging methods is briefly discussed.

Subject headings: Instrumentation: AO - planetary systems - stars: imaging

Suggested running page header: Angular Differential Imaging

1. Introduction

Direct detections of very faint exoplanets and brown dwarfs near bright stars are essential to understand substellar formation and evolution around stars. This endeavor is now one of the major goals for next generation 10-m telescope instruments and future 30- to 100-m telescopes. The task is dauntingly difficult. The exoplanet or brown dwarf image is usually

---

much fainter than the background from the brilliant stellar point spread function (PSF) image. Besides the Poisson noise limit, ground-based telescopes suffer from atmospheric turbulence that produces random short-lived speckles that mask faint companions. If these two limitations were the only ones, a simple solution would be to integrate longer to average these random noises and gain as the square root of the integration time. But observations have shown that, for integrations longer than a few minutes, the PSF noise converges to a quasi-static noise pattern, thus preventing a gain with increasing integration time (Marois et al. 2003, 2005; Masciadri et al. 2005). To achieve better detection limits, it is thus necessary to subtract the quasi-static noise using a reference PSF. Both ground- and space-based imaging are plagued with this stellar PSF calibration problem caused by imperfect optics and slowly evolving optical alignments. For ground-based imaging, subtraction of a reference PSF obtained from a star close to the target achieves a factor ~ 4 of PSF noise attenuation, leaving residuals that are also quasi-static and thus severely limiting detection of fainter companions (Marois et al. 2005). For space telescopes that have a better PSF stability, like HST, a partial solution was found by subtracting two stellar images acquired during the same orbit with a different roll angle. This technique, called "roll deconvolution", successfully subtracts the stellar image by a factor 50 (Schneider & Silverstone 2003) but is also ultimately limited by PSF evolution. A similar technique, called angular differential imaging (ADI), can be used on ground-based altitude/azimuth telescopes to subtract a significant fraction of the stellar quasi-static noise and can potentially achieve detection limits that improve as the square root of the integration time.

In this paper, the ADI technique is described and its performances is analyzed using a simple analytical model and Gemini Altair/NIRI data. The PSF stability with Altair/NIRI is studied and its impact on ADI performances is discussed. Detection limits for three stars of our ongoing young nearby star survey are then shown. A comparison between ADI and classical observations is also presented. Finally, the possibility of using ADI with other

high-contrast imaging techniques is discussed.

2. The Angular Differential Imaging Technique

ADI is a PSF calibration technique that can, in principle, suppress the PSF quasi-static structure by a large factor (Marois 2004). It consists of the acquisition of a sequence of images with an altitude/azimuth telescope and the instrument rotator turned off (at the Cassegrain focus) or adjusted (Nasmyth) to keep the instrument and telescope optics aligned. This setup improves the stability of the quasi-static PSF structure throughout the sequence while it causes a slow rotation of the field of view (FOV) with respect to the instrument. For each image, a reference PSF obtained from other images in the sequence is subtracted to remove the quasi-static structure. Given enough FOV rotation during the sequence, this subtraction preserves the signal from any eventual companion. All the image differences are then rotated to align the FOV and are median combined.

This technique offers a number of advantages over more classical ground-based observations since the target observations themselves are used to construct a reference PSF. This means that the reference PSF has the same spectrum and brightness as the target and that no time is lost to acquire reference observations of a different target. Ghost images from optical reflections and the sky flux are also removed by the subtraction. The detector flat field errors are averaged since each image difference needs to be rotated to align the FOV, the field is thus integrated with different pixels as it rotates on the detector. The ADI technique is a generalization of the "roll deconvolution" technique used with HST since several images each at a different field angle are acquired and combined. A technique similar to ADI has been developed independently by Liu (2004) to search for circumstellar disks.

3. Noise Attenuation Theory with ADI

For each image of an ADI sequence, a reference PSF has to be built from images of the same sequence. The way that this reference PSF is built is of great importance since it directly affects the noise attenuation performance. We have used two methods to construct the reference PSF.

The first method is simply to take the median of all the images of the sequence. If enough field rotation has occurred during the sequence so that an eventual point source has moved by at least twice its full width at half maximum (FWHM), then this point source will be largely rejected by the median which will leave only the average telescope and instrument PSF. The minimum distance at which this occurs is noted R_{min}. Since the median is taken over a large number of images, the pixel-to-pixel noise (i.e. PSF, flat field, dark and sky Poisson noises and detector readout noise) of the reference image is much less than that of any individual image. Thus this first method minimizes the noise in regions where the residuals are limited by pixel-to-pixel noise. However, since a sequence typically lasts more than an hour, the reference PSF only has modest quasi-static speckle correlation with the individual images of the sequence.

The second method is to take the median of only a few images as close in time as possible but for which the displacement due to field rotation at a given separation is at least 1.5 PSF FWHM. This displacement ensures that the flux inside the PSF core of an eventual point source is not significantly reduced by the subtraction. The time τ_{min} required for such field rotation is function of the separation angle from the target, the target azimuth A and zenith distance z and the telescope latitude ϕ. The rotation rate ψ (degree/minute) of the FOV is obtained from the time derivative of the parallactic angle and is given (McLean 1997) by

$$\psi = 0.2506 \frac{\cos A \cos \phi}{\sin z} \tag{1}$$

Figure 1 is provided as a reference to determine τ_{min} for observations from the summit of the Mauna Kea. This second technique provides stronger quasi-static speckle noise attenuation since the reference PSF is built using images acquired at short time intervals. However, the pixel-to-pixel noise of the reference image may not be negligible compared to that of an individual image.

The first method is optimized for regions where the residuals are limited by pixel-to-pixel noise while the second is optimized for regions where the residuals are still limited by speckle noise. The combination of both techniques into a single reduction algorithm will be discussed in section 5.2.

The ADI technique attenuates the PSF noise in two steps: (i) by subtraction of a reference image to remove correlated speckles and (ii) by the combination of all residual images after FOV alignment to average the residual noise. The noise attenuation $N/\Delta N$ is defined as the local noise N in an image over the residual noise ΔN of a difference image.

The noise attenuation obtained by the subtraction of the reference PSF, $[N/\Delta N]_{\mathrm{S}} (\theta, \tau, t_{\mathrm{exp}})$, is a function of the angular separation, θ, the time interval τ between the original and the reference image and the individual image exposure time t_{exp} (neglecting overheads). Strong quasi-static speckle correlation between successive images leads to strong attenuation and thus better detection limits for a given total integration time.

For simplicity, if we assume a single quasi-speckle source evolving over a single timescale τ_{speck}, the speckle attenuation resulting from the combination of all difference images is function of the PSF speckle evolution timescale τ_{speck}. Its behavior can be defined for two limiting regimes: a) when either τ is much shorter or much longer than τ_{speck} and b) τ is of

the order of τ_{speck}.

In the first regime, the residuals of consecutive image differences are decorrelated, either because the correlated structure of the PSF which lasts for long times has been removed, leaving only Poisson noise, or because the PSF structure was already uncorrelated between consecutive images in the first place. If this is the case, assuming Gaussian statistics, the speckle attenuation increases with the square root of the total number of image differences. For a sequence of time t, the final noise attenuation $N/\Delta N$ is simply

$$\frac{N}{\Delta N}(t, \theta, \tau, t_{\mathrm{exp}}) \cong \sqrt{\frac{t}{t_{\mathrm{exp}}}} \left[\frac{N}{\Delta N} \right]_{\mathrm{S}} (\theta, \tau, t_{\mathrm{exp}}) \qquad (2)$$

When τ is of the order of τ_{speck}, all differences show only partially correlated residuals since they are separated by a time of the order of the evolution timescale of the PSF structure. For t_{exp} shorter than τ, the residuals of consecutive differences are correlated and do not average-out as efficiently as in the optimistic regime. Assuming that only the noise having a spatial scale ~ 1 PSF FWHM limits point source detection, the time needed to decorrelate this noise will be the shortest time between τ_{min} and τ_{speck}. The final noise attenuation $N/\Delta N$ is thus

$$\frac{N}{\Delta N}(t, \theta, \tau, t_{\mathrm{exp}}) \cong \sqrt{\frac{t}{\mathrm{MIN}(\tau_{\mathrm{min}}, \tau_{\mathrm{speck}})}} \left[\frac{N}{\Delta N} \right]_{\mathrm{S}} (\theta, \tau, t_{\mathrm{exp}}). \qquad (3)$$

We emphasize that ADI guarantees a gain in detection with increasing observing time for both regimes. In the worst case, the speckle attenuation efficiency is limited by field rotation. This is an enormous advantage over classical observation where no reference PSF is obtained in which the quasi-static aberrations prevent significant gain after a relatively short observing time. An equation similar to Eq. 3 also applies to classical observations, but in this case there is no τ_{min} since the field is not rotating. Speckle attenuation is then governed by τ_{speck},

which can be very large, reducing drastically the efficiency of the observations. Section 6.3 presents a comparison of ADI and classical observations.

4. Observations

The ADI technique was first used at the Gemini north telescope using the Altair adaptive optic system (Herriot et al. 1998) and NIRI (Hodapp et al. 2000) in queue mode. Observations and detailed results obtained for three stars of our nearby young star survey, Vega, HD18803 and HD97334B are presented. Data for two other stars, HIP18859 and HD1405 will also be discussed for comparison since they have been acquired with a different technique.

For Vega, HD18803 and HD97334B, the imaging sequence consisted in the acquisition of a series of saturated images in the off methane 1.58μm 6.5% bandwidth filter with the cassegrain rotator turned off. This filter was chosen to minimize the brightness ratio of the star to that of methanated exoplanets or brown dwarfs. Unsaturated short exposures were acquired before and/or after the saturated sequence to calibrate detection limits.

For Vega, data were obtained on 2004 August 26 and 2004 September 1 (program GN-2004A-Q-11). In total, 225 and 177 30s exposures were respectively acquired on the 26th and 1st. Because of Vega's brightness, short exposure PSFs of a nearby reference star were acquired for photometric calibration. Seeing conditions were excellent on the 26th and average on the 1st. Images were saturated inside a $\sim$6″ diameter. For HD18803, 90 30s exposures were obtained on 2004 December 24 (program GN-2004B-Q4) and, for HD97334B, 90 30s exposures were acquired on 2005 April 18 (program GN-2005A-Q16). For HD18803 and HD97334B, seeing conditions were average to good and PSFs were saturated inside diameters of 0.7″. Table 1 summarizes the observations. Strehl ratios were obtained by analysing unsaturated data acquired before and after each sequence and by comparing

the PSF peak intensity with that of a simulated unaberrated PSF having the same pixel sampling, bandpass and integrated flux. It can be deduced from table 1 that since R_{min} is less than the saturated radius for all three targets, ADI can be applied at all separations to detect point sources.

As part of Altair science verification we have obtained a sequence of observations of the star HIP18859 on 2003 November 18 (program GN-2003B-SV-102). During this sequence, the filter was switched from the broadband H filter to a narrow band filter every fourth exposure to acquire unsaturated images. This data set will be discussed in section 6.1.

Observations of the star HD1405 were obtained on 2004 August 23 (program GN-2004B-Q-14) with the instrument rotator operating to keep the FOV orientation fixed throughout the sequence. In total, 38 30s exposures were obtained. These observations will be used in section 6.3 for a comparison between ADI and classical observations.

5. ADI Data Reduction Algorithm

5.1. Preliminary Data Reduction

The data reduction consists of flat field normalization, bad pixel correction using a median over surrounding pixels, and distortion correction using software provided by the Gemini Staff (Trujillo, private communication) and modified to use the IDL *interpolate* function with cubic interpolation. Images were then copied into larger blank images to ensure that no FOV is lost when shifting and rotating images. The center of the PSF of the first image of the sequence was then registered to the image center by minimizing the diffraction spikes residuals after subtraction of a 180-degree rotation of the image. The rest of the images were then registered by cross-correlation of the diffraction spikes with the first image. An azimuthally symmetric intensity profile was finally subtracted from each image

to remove the smooth seeing halo.

5.2. ADI algorithm

As discussed in section 3, two methods can be used to subtract the quasi-static PSF structure: subtracting the median of all images or subtracting a reference PSF obtained from a few images acquired as close in time as possible. These two methods can be combined into a single algorithm that optimizes speckle subtraction and minimizes pixel-to-pixel noise. First, the median of all the images is subtracted from each individual image. An optimized reference PSF (second method) is then obtained for each image by median combining 4 images (two acquired before and two after) that have at least 1.5 λ/D field rotation. This choice insures that the average τ of the reference PSF is ~ 0. For the construction of this reference PSF, the image is broken into many 30 pixels wide annuli to accommodate for the dependence of τ_{min} on the separation. The intensity of the reference PSF is then scaled appropriately inside each annulus to minimize the rms noise after subtraction. The scaling factor converges to zero if the annulus is dominated by pixel-to-pixel noise or to unity if it is dominated by correlated speckles. The optimized reference PSF is then subtracted and the difference is rotated to align the FOV to that of the first image. Finally, a median is taken over all differences. Optionally, the final residual image may be convolved by a Gaussian of FWHM equal to that of the PSF to attenuate further the high frequency noise. Table 2 summarizes the entire ADI reduction algorithm.

6. Results

6.1. PSF Evolution Time-Scale

The PSF noise evolution timescale can be studied through the evolution of the noise attenuation $[N/\Delta N]$ for the difference of two images as a function of the time interval, τ. The noise attenuation is the ratio of N and ΔN, which are the measured rms noises in an annulus of width equal to one PSF FWHM in the original and in the difference images respectively. For this analysis, all images have first been unsharp masked using a 25×25 box to remove low-frequency noise and then median filtered with a 4×4 box to remove hot/bad pixels. This step is necessary to prevent biasing the noise estimate N of single images and leaves only speckles that have a spatial scale of the order of λ/D. Images were subtracted two by two with increasing time interval. Fig. 2 shows the noise attenuation for Vega, HD18803 and HD97334B for angular separations of 2, 4, 6 and 8 arcsec.

All noise attenuation curves show stronger noise attenuation for shorter time intervals. For HD18803 and HD97334B, the noise attenuation reaches $\sim 2 - 5$ inside 4 arcsec for $\tau \sim 2$ minutes. At larger separation, the residuals are limited by pixel-to-pixel noise. For separations less than 4 arcsec, the noise attenuation drops by a factor 2 after approximately 60 minutes. For Vega, the noise attenuation reaches $\sim 4 - 6$ at all separations for $\tau \sim 1$ minutes and drops by a factor 2 after approximately 15 to 20 minutes. The stronger noise attenuation achieved on Vega and HD97334B for short time intervals could be explained by better seeing that stabilizes the structure and enables a better subtraction. Additionally, since $\tau_{\min}$ is less than 10 minutes at $1''$ within ± 1h from the meridian for all targets having a declination $-30°$ to $+65°$ at Mauna Kea (see Fig. 1), ADI can be used with little loss of speckle attenuation ($\sim 30\%$) on most of the available sky for separations greater than $\sim 0.5''$ and $H \sim 5$ stars.

Analysis of the HIP18859 data set that included a frequent filter change to acquire unsaturated images shows that a drop by a factor of 2 in speckle attenuation occurs following each filter change. This evolution of the PSF structure is probably due to the filter wheel not returning to its exact position after each change. This suggests that the best observing procedure is to prevent any alteration of the optical setup during an observing sequence to maximize the PSF noise stability.

6.2. Contrast Performances

Fig 3 shows for all ADI targets the noise attenuations $[N/\Delta N]_\mathrm{S}$ achieved in average for each image differences and the one obtained $[N/\Delta N]$ after median combining all image difference. Again, a 25×25 pixels unsharp mask and a 4×4 pixels median filter were applied to each image to produce this figure. A total noise attenuation of ~ 35 between 2 and 10 arcsec was obtained for HD18803 and HD97334B, while this attenuation reached 100 for Vega (August 26th data). The higher attenuation for Vega comes partly from the larger number of images (225 *vs* 90) and partly from better seeing conditions which provided a better attenuation from single image subtractions. For separations greater than $2''$, all three targets achieve more than 70% of the $\sqrt{n}$ attenuation expected if residuals are decorrelated. HD97334B and HD18803 noise attenuations are shown to improve at all separation down to the detector saturation limit and clearly below it if we extrapolate the performances shown at $0.7''$. To our knowledge, this is the first time that such behavior is clearly demonstrated for an acquisition and reduction technique designed for speckle attenuation. The wall raised by quasi-static speckles that prevents a gain with longer integration time for standard observing techniques (Marois et al. 2003, 2005; Masciadri et al. 2005) can thus be removed by ADI.

Fig. 4 shows detection limits (5σ) in magnitude difference as a function of angular separation obtained with the ADI technique for all three ADI targets. To produce this figure,

data were reduced following the procedure explained in section 5.1. No unsharp masks were used for the ADI reduction since multiple tests have showed that even if they removed the low-frequency spatial noise, they did not increase candidates S/N and were slightly biasing the photometry. The detection limits are calculated using the ratio of the unsaturated PSF maximum and the noise in the residual image as a function of angular separation. The noise is calculated inside annuli of increasing diameter and width equal to 1 PSF FWHM. Both the unsaturated PSF and residual images are convolved by an aperture of diameter 2 PSF FWHM prior to this calculation; the unsaturated PSF is also flux normalized to account for exposure time differences. Finally, detection limits were corrected for the Altair estimated anisoplanatism following the Strehl S equation found in the Gemini web page[4]

$$S(\theta) = S_0 e^{-\left(\frac{\theta}{12.5}\right)^2} \tag{4}$$

where θ is expressed in arcsec. The detection limits obtained with the ADI technique on Vega at separations greater than $\sim 5''$ is two orders of magnitude deeper than the Palomar H-band image (Metchev et al. 2003) and approximately a factor of ten deeper than the Keck K-band image of (Macintosh et al. 2003). Although the ADI technique is inherently optimized for relatively large separations, the good Gemini PSF stability enables excellent performances at sub-arcsec separations. Indeed, the ADI contrast of $\Delta m = 10.5 - 11.2$ (5σ) at $0.7''$ obtained on HD18803 and HD97334B equals the $\Delta m = 10.8$ (5σ) at $0.7''$ obtained with the simultaneous differential imaging (SDI) VLT camera optimized for multi-wavelength speckle suppression (Biller et al. 2006). This shows the potential of ADI to achieve high-contrast detection using a simple, yet efficient, observing technique with standard instruments. Two faint sources were detected around Vega, three were detected around HD18803 and one around HD97334B. Analysis of these sources are left for future papers (Doyon et al. and

[4]http://www.gemini.edu/sciops/instruments/altair/altairIndex.html

Lafrenière et al., in preparation). Fig. 5 illustrates the noise attenuation obtained for Vega (August 26th) using the ADI technique.

Mass limits corresponding to these observations, corrected for the filter use,[5] are estimated using evolutionary models of Baraffe et al. (2003) assuming ages of 350, 45 and 85 Myr for Vega, HD18803 and HD97334B, respectively (Song et al. 2001; Montes et al. 2001). Both HD18803 and HD97334B achieve detection limits of 1-2 $M_{\rm Jup}$ at $3''$ (60 AU for both targets), while $\sim$3 $M_{\rm Jup}$ is obtained for Vega at $7''$ (55 AU). The ADI technique is thus well suited to survey jovian companions at intermediate separations (50-300 AU) orbiting young nearby stars.

6.3. Comparison between ADI and Classical Observations

In the previous sections it was shown that the ADI technique can achieve high contrast given a sufficiently long integration time and good PSF stability. To compare the performances of ADI and classical observations we analyze the first 38 images of the HD97334B ADI sequence and the 38 images of the HD1405 "classical" sequence. For this analysis, both data sets have been reduced according to section 5.1. Furthermore, a 25×25 pixels unsharp mask was applied to all images to remove the low spatial frequency quasi-static noise. Then a 4×4 pixels median filter was applied to all images to remove the bad/hot pixels. These steps are performed here only to bring the classical observations on even ground with ADI in order to study the evolution of the noise at spatial scales that most severely limit point source detections. For the HD97334B sequence, images differences were obtained according to section 5.2; these differences were then rotated to align the FOV to that of the first image.

---

[5]The star-to-planet brigthness ratio is reduced by a factor $\sim$2.6 when using a 6.5% bandpass methane filter instead of a broad band H, as derived from a theoretical spectrum of Allard et al. (2001).

An increasing number of images (differences for HD97334B) of both sequences were median combined to study the noise attenuation as a function of the total observing time at $2''$, the results are presented in Fig. 6. The ADI reduction technique achieves 80% of the maximal square root gain (Eq. 2) compared to less than 20% for HD1405 data. For this example, ADI achieves 4 times better noise attenuation, it is thus at least 16 times more efficient. The small deviation from the expected $\sqrt{n}$ speckle attenuation ADI gain might be coming from seeing variations and/or slowly evolving speckles that are producing, after partial subtraction from the reference PSF, partially correlated speckles (see Eq. 3) or uncorrelated speckles having non Gaussian noise statistics (Marois 2004; Soummer & Aime 2004).

7. Discussion

ADI is a general high-contrast imaging technique that can be applied to any existing or upcoming large altitude/azimuth telescope. It is also flexible enough to be combined with a number of other high-contrast imaging techniques.

ADI performances at small separations ($< 1''$) require long time intervals and thus suffer from important PSF variations that prevent good quasi-static speckle attenuations. These variations may come from uncorrected atmospheric turbulence, variable seeing and slowly evolving quasi-static aberrations from the telescope and instrument optics. The use of a multi-wavelength instrument (Marois et al. 2000; Doyon et al. 2004; Lafrenière et al. 2004; Marois et al. 2004, 2005; Biller et al. 2004) or an IFU (Sparks & Ford 2002) to acquire simultaneous images at multiple wavelengths across the methane absorption bandhead at 1.6 μm (the simultaneous spectral differential imaging (SSDI) technique, see Racine et al. (1999); Marois et al. (2000); Biller et al. (2004); Marois (2004); Marois et al. (2005)) could provide good short-lived speckle attenuation and increase detection limits. It has been

shown that such instruments are ultimately limited by non-common path aberrations, which are expected to be stable over long periods of time as they come almost entirely from the instrument itself (Marois et al. 2005). Hence, the ADI technique nicely complements SSDI since it can be used to subtract the residuals caused by the non-common path aberrations.

Future high-contrast instrumentation for 8-10 m class or larger telescopes based on high-order adaptive optics (AO) systems (Macintosh et al 2004; Mouillet et al. 2004) will most likely improve the stability of the PSF. Thus, if combined to such instruments, ADI could prove even more successful. These new AO systems will also provide the high Strehl ratios required to bring coronagraphy at the forefront of high-constrast imaging. However, even a very good coronagraph cannot totally suppress the light from uncorrected quasi-static wavefront errors and some level of quasi-static speckle noise will inevitably be present in coronagraphic observations. ADI would be a nice addition to coronagraphy as it could attenuate those residual speckles.

Ideally, all the techniques mentioned above, ADI, SSDI, high-order AO and coronagraphy, could be used together to form an extremely powerful tool to detect exoplanets and brown dwarfs around stars.

8. Conclusion

The ADI observing technique was described and its performance using Altair/NIRI at Gemini were presented. It was shown that faint companions can generally be detected with better S/N when compared to classical observing techniques for a wide range of declinations. The ADI technique produces a reference PSF from the same target imaging sequence, removing the need to move to a nearby star for PSF calibration or to acquire sky exposures (for H-band imaging). Since the reference PSF is built using images acquired minutes apart,

the reference PSF shows a good quasi-static speckle correlation.

The stability of the PSF plays a crucial role in ADI as it not only determines the speckle attenuation from the reference image subtraction but it also determines the regime in which the noise is attenuated with increasing observing time. It was reported that at Gemini with Altair/NIRI using 30s exposures, the PSF evolves on timescales of $\sim 10 - 60$ minutes and the attenuation by subtraction of a reference image reaches $\sim 2 - 6$ for short time intervals, achieving better speckle attenuation with better seeing conditions. The observations of HIP18859, for which a filter change during the sequence reduced significantly the speckle attenuation, underscore the importance of maintaining the optical setup fixed during the sequence. It was shown that the gain in S/N with increasing total observing time for separation greater than $2''$ reaches more than 70% of the optimal case, indicating that the noise is mostly decorrelated between residual images for these separations. ADI thus guarantees a large gain with longer observation sequences.

The noise attenuation obtained on Vega was 100, reaching a contrast of $\sim$20 magnitudes at $6''$ separation (47 AU). Observations of the young stars HD18803 and HD97334B yielded detection limits in difference of magnitude of 10.5-11.2 at $0.7''$, similar to the SDI camera at VLT (Δm of $\sim$10.8 at $0.7''$), which is an optimized speckle suppression instrument. When combined to substellar models and estimated age for these stars, these observations show that ADI is well suited to search for jovian companions having a mass greater than 1-2 M_{Jup} 50-300 AU away from nearby young stars. Finally, ADI could easily and advantageously be combined with SSDI, high-order AO and coronagraphy to improve the detection limits of exoplanets and brown dwarfs at all separations.

REFERENCES

Allard, F., Hauschildt, P. H., Alexander, D. R., Tamanai, A., Schweitzer, A. 2001, ApJ, 556,357

Baraffe, I., Chabrier, G., Barman, T. S., Allard, F., Hauschildt, P. H. 2003, A&A, 402, 701

Biller, B. A., Close, L.,Lenzen, R., Brandner, W., McCarthy, D., Nielsen, E., Hartung, M. 2004, Proc. SPIE, 5490, in Press

Biller, B. A., Close, L., Masciadri, E., Lenzen, R., Brandner, W., McCarthy, D., Henning, T., Nielsen, E., Hartung, M. 2006, IAUC 200 proceedings, in press

Doyon, R., Lafrenière, D., Marois, C., Racine, R., Nadeau, D. 2004, Proc. SPIE, 5382, 21

Herriot, G., Morris, S., Roberts, S., Fletcher, J. M., Saddlemyer, L. K., Singh, G., Véran, J., Richardson, E. H. 1998, Proc. SPIE, 3353, 488

Hodapp, K., Hora, J., Graves, E., Irwin, E. M., Yamada, H., Douglass, J. W., Young, T. T., Robertson, L. 2000, Proc. SPIE, 4008, 1334

Koerner, D. W., Sargent, A. I., Ostroff, N. A. 2001, ApJL, 560, 181

Lafrenière, D., Doyon, R., Racine, R., Marois, C., Nadeau, D. 2004, Proc. SPIE, 5492, 500.

Liu, M. C. 2004, Science, 305, 1442

Luhman, K. L., Jayawardhana, R. 2002, ApJ, 566, 1132

Macintosh, B. A., Becklin, E. E., Kaisler, D, Konopacky, Q., Zuckerman, B. 2003, ApJ, 594, 538

Macintosh et al. 2004, Proc. SPIE, 5490, 359

Marois, C., Doyon, R., Racine, R. & Nadeau, D. 2000 PASP, 112, 91

Marois, C., Doyon, R., Racine, R., Nadeau, D. 2003, Astronomy with High Contrast Imaging: From Planetary Systems to Active Galactic Nuclei (eds. C. Aime and S. Soummer), 8, 233

Marois, C. 2004, PhD. thesis, Université de Montréal

Marois, C., Racine, R., Doyon, R., Lafrenière, D., Nadeau, D. 2004, ApJ, 615, L61

Marois, C., Doyon, R., Racine, R., Nadeau, D., Riopel, M., Vallée, P., Lafrenière, D. 2005 PASP, 117,745

Masciadri, E., Mundt, R., Henning, Th., Alvarez, C., Barrado y Navascus, D. 2005, ApJ, 625, 1004

McLean, I. S., Electronic Imaging in Astronomy: Detectors and Instrumentation, Wiley, 1997, ch.3

Metchev, S. A, Hillenbrand, L. A., White, R. J. 2003, ApJ, 582, 1102

Montes, D., López-Santiago, J., Gálvez, M. C., Fernández-Figueroa, M. J., De Castro, E., Cornide, M. 2001, MNRAS, 328, 45

Mouillet, D., Lagrange, A. M., Beuzit, J.-L., Moutou, C., Saisse, M., Ferrari, M., Fusco, T., Boccaletti, A. 2004, ASP Conf. Ser., 321, 39

Racine, R., Walker, G. A. H., Nadeau, D., Doyon, R., Marois, C. 1999, PASP, 111, 587

Schneider, G., Silverstone, M. D. 2003, Proc. SPIE, 4860, 1

Song, I., Caillault, J.-P., Barrado y Navascués, D., Stauffer, J. R. 2001, ApJ, 546, 352

Soummer, R., Aime, C. 2004, Proc. SPIE, 5490, 495

Sparks, W. B., Ford, H. C. 2002, ApJ, 578, 543

Table 1: Observations

Object	Date	Nb images	Field rotation (degree)	$R_{\min}$ ($''$)	$\tau_{\min}$ (min) at meridian	Strehl
Vega	August 26, 2004	225	99	0.15	4	0.24[a]
Vega	September 1, 2004	177	69	0.1	4	0.12
HD18803	December 24, 2004	90	99	0.15	1	0.10
HD97334B	April 18, 2005	90	54	0.3	4	0.16

[a] Short exposures for the August 26th run are saturated. Since the September 1st short exposures fill 55% of the pixel electron well at the PSF peak intensity, it is approximated that the Strehl ratio for August 26th is at least 2 times higher than the one estimated for September 1st.

Table 2: ADI Data Reduction Algorithm

Reduction	Flat field normalization	
	Bad pixel correction	
	Distortion correction	
	Copy in bigger blank image	
Processing	Image registration	
	Radial profile subtraction	
	Diffraction spikes & saturation mask	
ADI	Subtraction of the median of all images	
	For each 30-pixel wide annulus	Find 4 images with $\tau \geq 1.5\tau_{\min}$
		Median combine these 4 images
		Flux normalization
		Subtract reference annulus
	Calculate parallactic angle	
	Rotate images	
Coaddition	Median combination of all differences	
	(optional) Convolution by Gaussian	
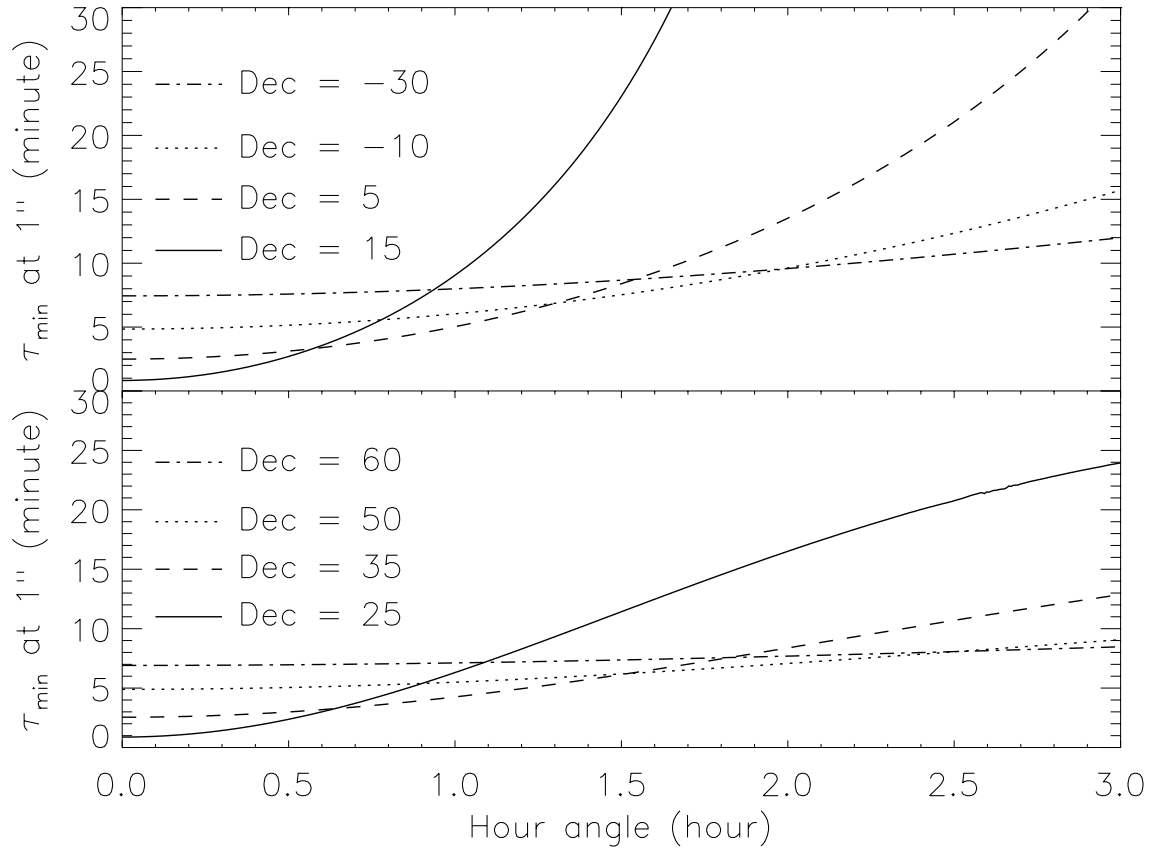
Fig. 1.— Interval of time required for a point source to move by 1 λ/D (1.6μm on a 8-m diameter telescope) at 1″ as a function of hour angle for various declinations. Calculated for Mauna Kea, Hawaii.
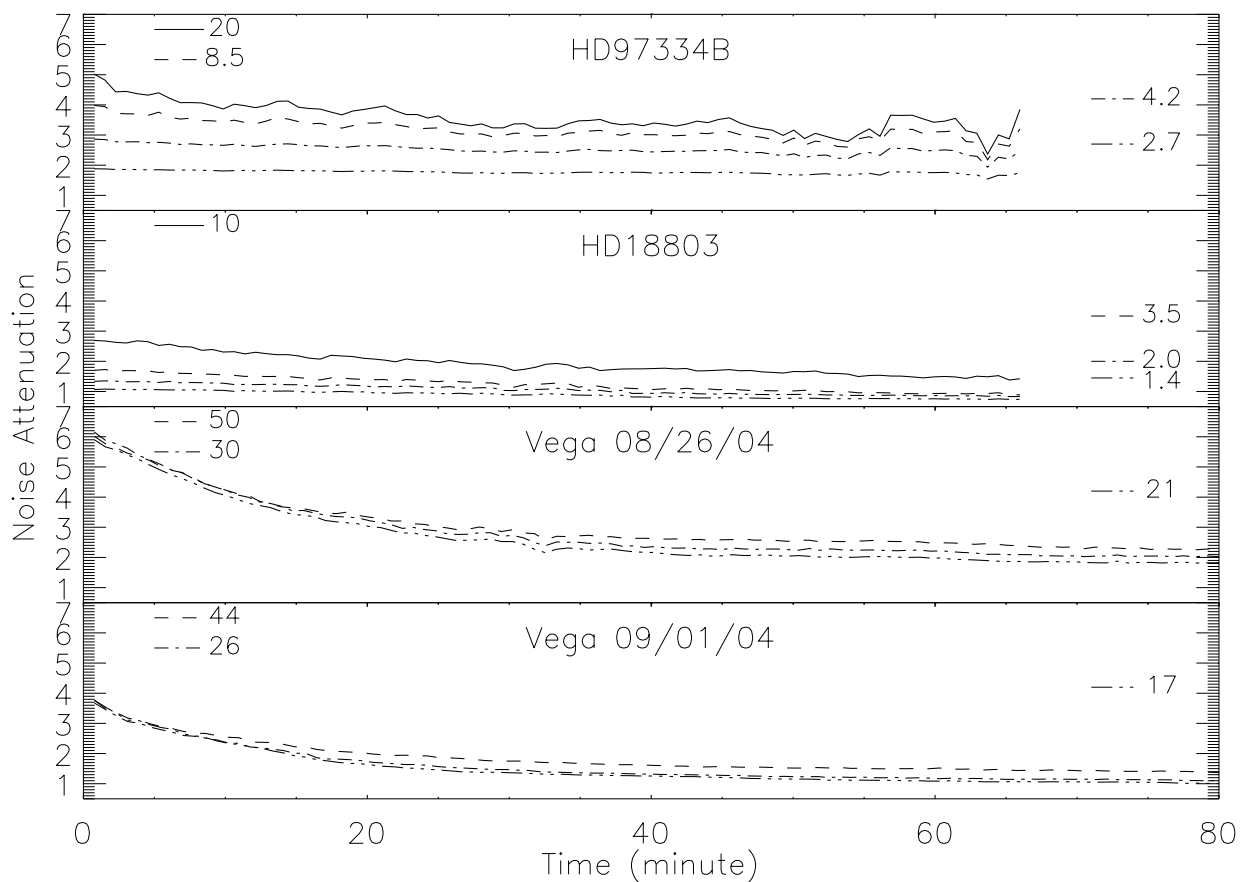
Fig. 2.— Noise attenuation obtained by subtracting images two by two with increasing time interval for HD97334B, HD18803 and Vega acquired on the 26/08/04 and on the 01/09/04. Solid, dashed, dot-dashed and tripe dot-dashed lines are for 2″, 4″, 6″ and 8″ respectively. For Vega, there is no solid line for 2″ since images are saturated at that separation. Small lines show the estimated noise attenuation limit imposed by photon, sky, read and dark noises.
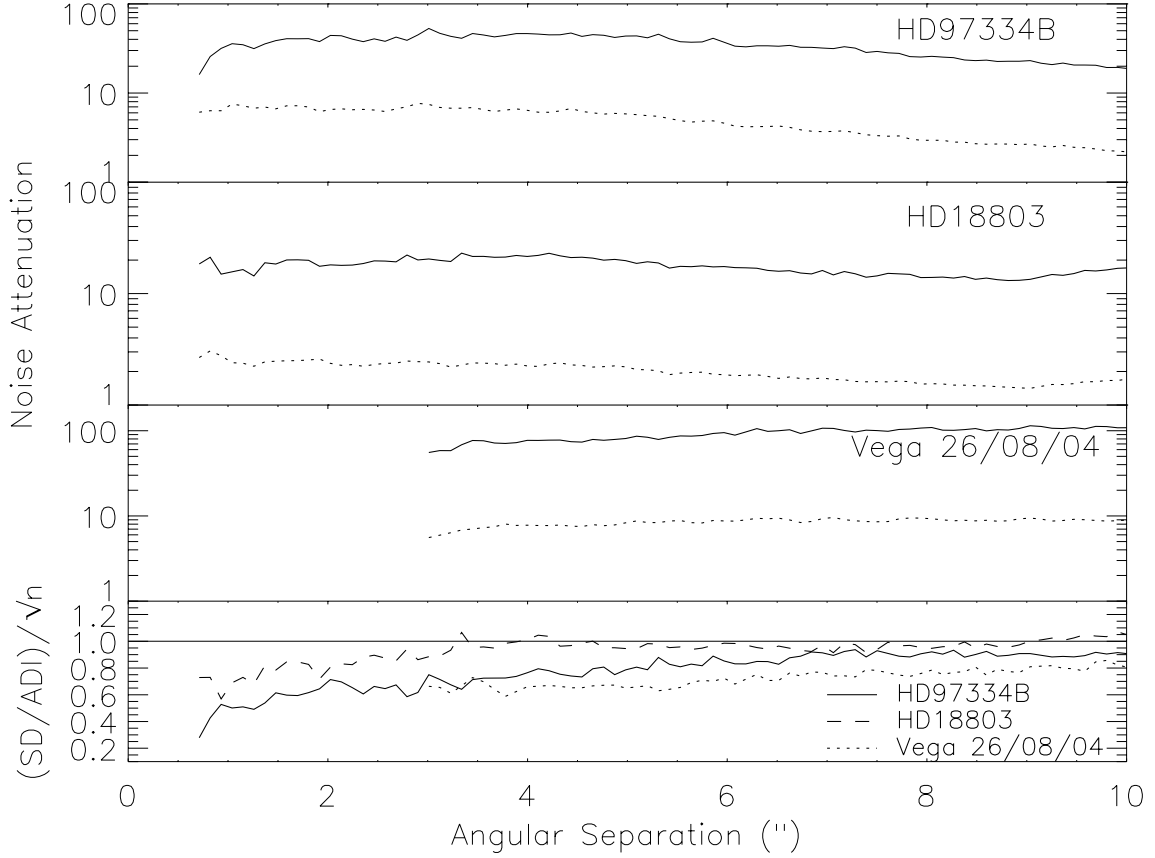
Fig. 3.— Single ADI difference $[N/\Delta N]_\mathrm{s}$ and total ADI $[N/\Delta N]$ noise attenuations with separation for HD97334B, HD18803 and Vega. Dotted lines show attenuation from a single ADI difference while solid lines show the attenuation after median combining all ADI differences. The bottom panel shows the attenuation ratio of a single ADI difference SD and the one obtained from combining all ADI differences ADI divided by the square root of the total number n of images in each sequence.
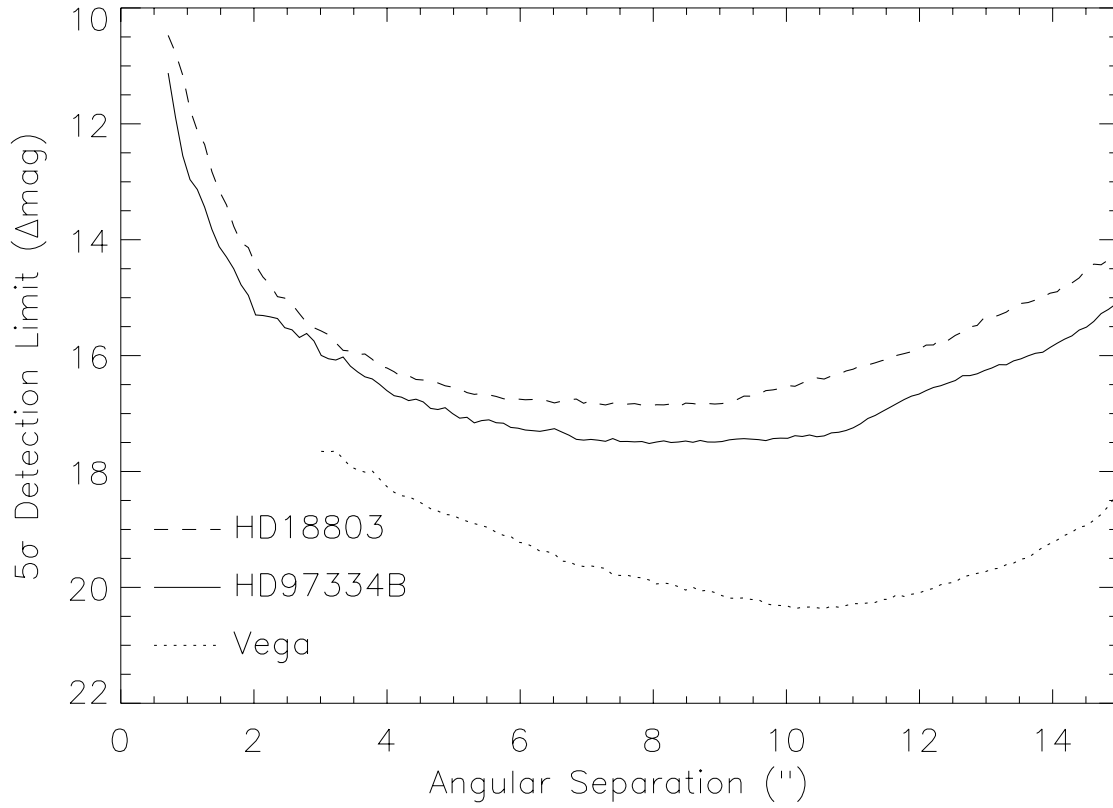
Fig. 4.— Detection limits (5σ) as a function of angular separation for HD18803, HD97334B and Vega (August 26th). The three curves are bended upward for separations greater than $9''$ due to the Altair anisoplanatism correction.
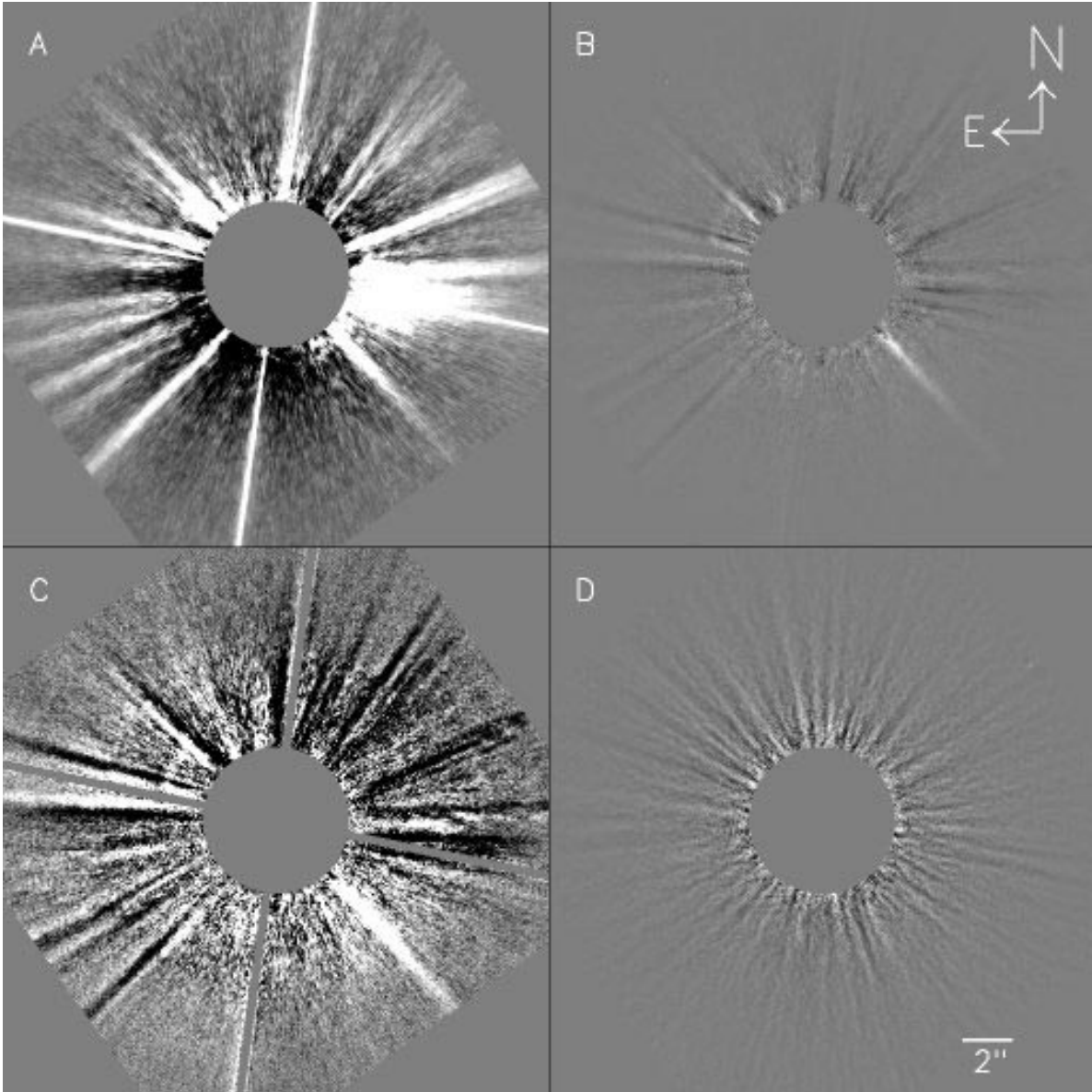
Fig. 5.— Vega (August 26th) ADI data reduction. A: A single image after flat field normalization, bad pixel correction, distortion correction, registering and removal of an azimuthally symmetric profile. FOV is $22'' \times 22''$ using a linear intensity range of $\pm 10^{-6}$ from the estimated PSF peak intensity. B: A single ADI difference image shown with the same intensity range. C: same as B with an intensity range 25 times smaller. D: The final combination of all ADI differences shown with the same intensity range as C.
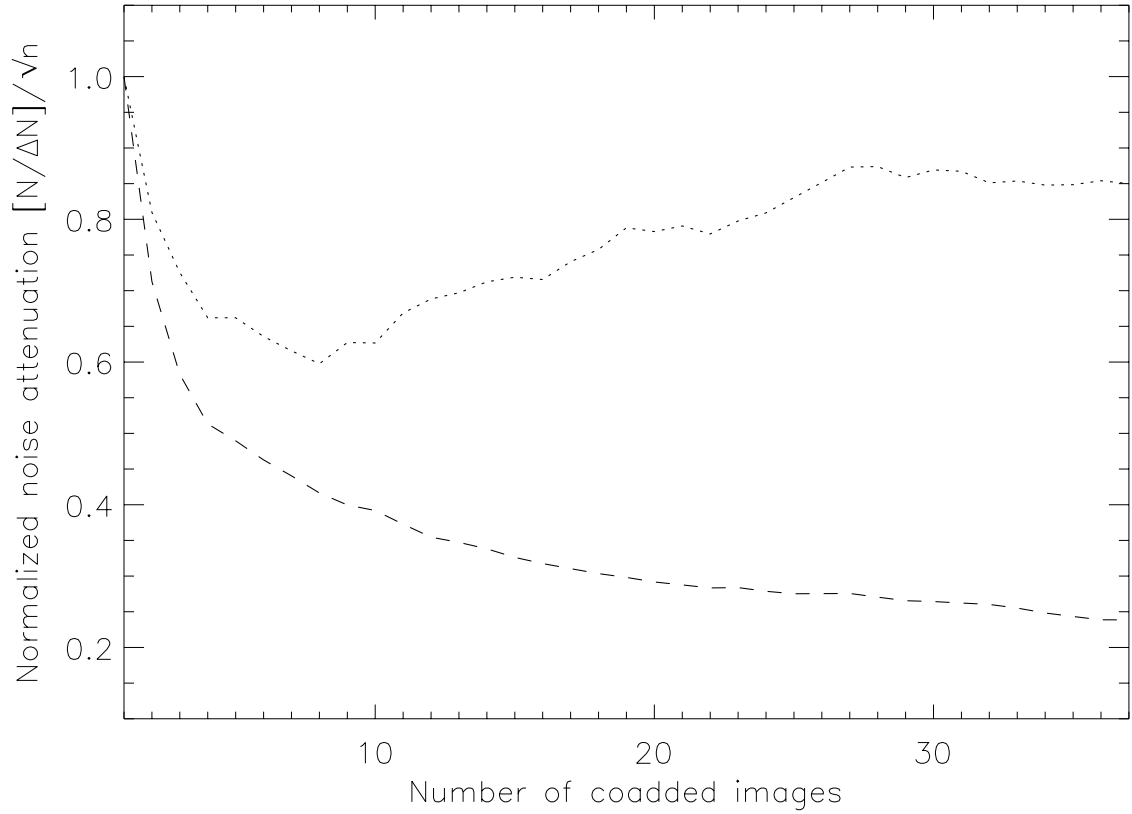
Fig. 6.— Normalized noise attenuation from the median combination of an increasing number of images (differences in the ADI case) at $2''$ separation. The dotted and dashed lines are respectively for the ADI reduction and the HD1405 without field rotation sequence. See section 6.3 for more details.